Journal of the European Ceramic Society 19 (1999) 1949–1959

PII: S0955-2219(99)00018-7
0955-2219/99/$ - see front matter

Spinel Fibers from Carboxylate Precursor

Yin Liu* and Richard M. Laine

Departments of Materials Science and Engineering, Chemistry, Macromolecular Science and Engineering Center, University of Michigan, Ann Arbor, MI, 48109-2136, USA

(Received 17 September 1998; accepted 22 January 1999)

Abstract

A spinel precursor was synthesized from a 1:2 stoichiometric mixture of $Al(O_2CH)_3{\cdot}3H_2O$ and $Mg(O_2CCH_3)_2{\cdot}4H_2O$ dissolved in H_2O with stabilizing additives. The precursor, as well as individual compounds were characterized using TGA, DTA, DRIFTS and XRD techniques to establish decomposition profiles. During pyrolysis, $Mg(O_2CCH_3)_2{\cdot}4H_2O$ decomposes first to an amorphous oxide contaminated with minor amounts of carbonate. At 300°C, rock salt (MgO) crystallizes. The spinel precursor behaves like a separate compound and decomposes directly to crystalline spinel at ≈600°C without any evidence of phase separation. The spinel precursor is easily extruded or hand drawn to form well-defined green fibers. Extruded green fibers (20 μm dia.) were pyrolyzed at 300°C/2 h/air to remove carboxylate ligands, and then heated at 15°C/min to 1500°C/2 h/air to sinter. The mechanical strength of these fibers was evaluated using a bending test method. The final fibers are ≈10 μm in dia., with 1·2 ± 0·4 μm grain size and offer an average bend strength of 1·0 ± 0·4 GPa. © *1999 Elsevier Science Limited. All rights reserved*

Keywords: $MgAl_2O_4$, precursors: organic, fibers, strength, spinels.

1 Introduction

In the past two decades, various commercial ceramic oxide fibers have been developed to meet the requirements of high temperature engineering applications. For example, a variety of alumina fibers are widely available including Saffil (dia. ≈3 μm, 5% silica, ICI Ltd.),[1] Sumika (dia. ≈17 μm, 50% silica, Sumitomo Ltd.) and the Nextel series of alumina based fibers (3 M: 312, 440, and 610, 10–12 μm dia.)[1–6] All of these fibers are processed via chemical approaches. However, a number of these fibers have a lower melting phase present at grain boundaries, which can reduce their high temperature performance and limit their high temperature utility. To increase high temperature fiber performance, phase pure oxide fibers, including YAG, mullite, and zirconia, have been processed using chemical routes, e.g. via carboxylate or sol-gel precursors.[7–10]

Phase pure oxide fibers have also been produced using methods other than chemical processing, including edge-defined film-fed growth (EFG),[11] laser-heated-pedestal-growth (LHPG),[12] melt spin,[13] and a colloidal sols methods.[14] Unfortunately these methods lead to large diameter fibers, which are inconvenient for use in fiber-reinforced CMC because of their poor weavability and low strength.[1,15]

Although many oxide fibers can be processed successfully, optimal fiber compositions and properties vary considerably depending on the engineering application.[1,15] For example, Al_2O_3 fibers cannot be used in cordierite, a common matrix material for CMCs,[16–18] because at high temperatures, Al_2O_3 reacts with cordierite to form mullite, thus damaging composite integrity. One solution is to use a cordierite 'inert' fiber, e.g. spinel as the reinforcing phase.[18] Also, the Al_2O_3–MgO–SiO_2 ternary phase diagram shows that Al_2O_3 and MgO or $2MgO{\cdot}SiO_2$ (forsterite) cannot coexist, i.e. Al_2O_3 fibers cannot be used to reinforce MgO or forsterite matrices.[19,20] In contrast, spinel is stable in both MgO and forsterite, thus spinel fibers might be used as reinforcement.[21,22]

Spinel fiber can also be used in metal matrix composites (MMCs). For example, in alumina fiber reinforced aluminum alloy (AlSi12CuMgNi) matrix composites, alumina fibers react with Mg to form spinel, and degrade composite performance.[21] The use of spinel fibers in this alloy matrix system could avoid this problem. Spinel fibers have other potential engineering uses. For example, spinel has a higher melting point (2135°C) than alumina (2072°C), which makes it a desirable refractory material.[22]

*To whom correspondence should be addressed.

Spinel is also highly resistant to chemical attack.[23,24] With a low dielectric constant, spinel offers important properties for insulating materials in electronic and communication industries.[25] Thus, spinel fibers provide a possible materials selection for diverse engineering applications, e.g. spinel fiber reinforced spinel composites are of potential use in radomes.[26]

To date, the literature on spinel fibers is limited to studies on [110] single crystal fibers grown by the laser-heated floating-zone process.[27,28] The tensile strength of the [110] spinel fibers ($2{\cdot}14 \pm 0{\cdot}5$ GPa) is comparable with *c*-axis sapphire (≈2·7 GPa) and [111] YAG (≈0·9 GPa) at room temperature and high temperatures (at 1433°C, 0·6 GPa for spinel fibers, ≈0·5 GPa for YAG and ≈0·6 GPa for sapphire).[27] Creep tests at 1927°C and a stress of 218·5 MPa show that the 1% strain time for [110] spinel is 35 min (28 min delay period, the time at which spinel starts to creep), which is comparable to that of *c*-axis sapphire (31 min, with a 30 min delay period).[27] Note that the [110] fiber direction eliminates some slip systems, four {111} and two {100} slip planes, and reduces the shear stress for the primary {111}⟨110⟩ and secondary {110} ⟨110⟩ slip systems, thus offering better creep resistance than most other directions.

Polycrystalline spinel, with fine grain sizes (2–5 μm), displays poor creep resistance ($26{\cdot}3\times10^{-5}$ h^{-1} at 12·4 MPa 1300°C^{-1}). Large grain size (1–3 mm) spinel displays creep resistance ($0{\cdot}1\times10^{-5}$ h^{-1} at 12·4 MPa 1300°C) comparable to polycrystalline Al_2O_3 ($0{\cdot}13\times10^{-5}$ h^{-1} at 12·4 MPa 1300°C^{-1}).[19,26] But in practical use, it is unlikely that such large grain size materials will provide good ambient temperature mechanical properties.[19] It is also impossible to make spinel fibers with such a grain size, because desired fiber diameters are ≈20 μm.[7]

We describe here, a precursor route to inexpensive, polycrystalline spinel fibers. This work represents an extension of our recently described study on YAG fibers derived from yttrium/aluminum carboxylate precursors.[7] The YAG fibers offer bend strengths of $1{\cdot}7 \pm 0{\cdot}2$ GPa (room temperature). In the present paper we discuss the: (1) reactivity patterns of $Mg(O_2CCH_3)_2{\cdot}4H_2O$, and 1:2 (Mg:Al, spinel stoichiometry) mixtures of this compound with $Al(O_2CH)_3{\cdot}3H_2O$ during their pyrolytic transformation to phase pure MgO and spinel respectively; (2) studies on fiber processing; and (3) initial studies on the mechanical properties of spinel fibers.

2 Experimental

2.1 General procedures

Aluminum tri(sec-butoxide) was purchased from Chattem Chemicals Inc, and used as received. Isobutyric acid (99%) was purchased from Pfaltz and Bauer Inc. Magnesium acetate hydrate (98%), $Mg(O_2CCH_3)_2{\cdot}4H_2O$, was purchased from Morton Thiokol Inc. (Danvers, MA) and used as received. Ethylene glycol (99%) was purchased from J. T. Baker, Inc. (Phillipsburg, NJ). Formic acid (95–97%) was purchased from Aldrich Chemical Co. (Milwaukee, WI). All the experiments were conducted in air.

2.2 Synthesis and characterization of spinel precursor

2.2.1 Aluminum formate hydrate $Al(O_2CH)_3{\cdot}3H_2O$ [FW = 216·08]

$Al(O_2CH)_3{\cdot}3H_2O$ was synthesized by reaction between aluminum tri(sec-butoxide), H_2O and formic acid, HO_2CH, as described in Ref. 7. The $Al(O_2CH)_3{\cdot}3H_2O$ gave a TGA ceramic yield (Al_2O_3) of 23·6% at 1000°C, the same as theory.

2.2.2 Magnesium acetate hydrate $Mg(O_2CCH_3)_2{\cdot}4H_2O$ [FW = 214.46]

$Mg(O_2CCH_3)_2{\cdot}4H_2O$ was used as received. The TGA ceramic yield of MgO is 19·1% (1000°C/air), versus a theoretical value of 18·8%.

2.2.3 Preparation of spinel precursor solution

A 1:2 stoichiometric precursor solution, $Mg(O_2CCH_3)_2$: $2Al(O_2CH)_3$, was prepared by dissolving 9·78 g (46·3 mmol) $Mg(O_2CCH_3)_2{\cdot}4H_2O$ and 20·00 g (92·6 mmol) $Al(O_2CH)_3{\cdot}3H_2O$ in 700 ml of boiling H_2O, in a 1000 ml beaker. Formic acid (≈6 g), ethylene glycol (4 g), and isobutyric acid (1 g) were added to stabilize the solution. The solution was then heated on a hot plate with constant stirring to evaporate the solvent until its viscosity was suitable (determined empirically for each spinning dope) for hand drawing fibers (final volume ≈20 ml, ceramic yield ≈ 19·3% by TGA). Then ≈ 10 ml of spinel precursor solution was transferred into a 50 ml schlenk flask, and vacuum dried at 90°C (≈0·75 Torr) for 2 h. The dried precursor gave a TGA ceramic yield of 27·5% at 950°C (theory = 22 wt%). After grinding in an alumina mortar and pestle in air, the precursor was ready for bulk material studies.

2.3 Pyrolyses and characterization of the bulk precursor

2.3.1 Measurement of density

Density measurements were performed as described elsewhere.[7] Vacuum dried spinel precursor was ground and pressed into 12.8 mm dia. semi-transparent disks. The resulting pellet is assumed to be nearly 100% dense (optical microscopy shows no pores). The pellet dimensions were

measured (calipers) to determine the densities. Average densities are $1{\cdot}64 \pm 0.01$ g cm^{-3}.

2.3.2 Pyrolysis studies
Ground samples (1 g) of $Mg(O_2CCH_3)_2{\cdot}4H_2O$, and spinel precursor were placed in separate alumina boats, and heated (10°C min^{-1} in air) to selected temperatures followed by a 2 h hold. Pyrolyses <1000°C were run as described elsewhere.[7] Pyrolyses >1000°C were conducted in a 51314 Lindberg furnace, equipped with a Lindberg 59246-P Com controller.

2.3.3 Thermogravimetric analyses (TGA)
TGA studies were performed on a Hi-Res TGA 2950 Thermal Analysis Instrument (TA Instruments. Inc., New Castle, DE). Samples were loaded on a Pt sample pan. The TGA was ramped at 10°C min^{-1} to 1000°C at 'High-Res 4', with a 40 cc min^{-1} N_2 balance flow and a 60 cc min^{-1} air purge flow.

2.3.4 Differential thermal analyses (DTA)
DTA experiments were conducted on a DSC 2910 Differential Scanning Calorimeter (TA Instruments, Inc., New Castle, DE). DTA samples (10–20 mg) were loaded in a Pt crucible and heated at the same rate as the corresponding TGA Hi-Res sample rate, to 1500°C in dry air at a flow rate of 50 cc min^{-1}. The DTA reference was α-alumina (Aluminum Co. of America, Pittsburgh, PA).

2.3.5 Diffuse reflectance infrared Fourier transform spectroscopy (DRIFTS).
DRIFTS studies were performed using a Mattson Galaxy Series FTIR-3000 (Mattson Instruments, Inc., Madison, WI). The experimental details were described in an earlier paper.[7] Ground KBr crystal, 450 mg, from International Crystal Laboratories (Garfield, NJ) was used as background. A 2·7 mg sample (0·6 wt% of KBr) was mixed with KBr for each analysis. The IR sample chamber was kept under a constant N_2 purge. A minimum of 250 scans were collected for each sample at ± 4 cm^{-1} resolution. IR peak positions were identified using a standard peak searching program.

2.3.6 XRD studies of precursor pyrolysis products
The transformation of the precursors to crystalline products, as a function of processing temperature, was followed by XRD, using a Rigaku Rotating Anode Goniometer (Rigaku Denki Co. Ltd., Tokyo, Japan). Samples (40–80 mg) were prepared using the same procedures as for the DRIFTS samples. The working voltage and current for the XRD instrument were 40 kV and 100 mA respectively. Cu K_α ($\lambda = 1{\cdot}54$ Å) radiation with a Ni filter was used. Scans were continuous from 5 to 90° 2θ with a step scan of 10° 2θ min^{-1} and increments of 0·05° 2θ. Product peak positions and relative intensities were characterized by comparison with standard JCPDS files.

2.4 Fiber studies

2.4.1 Fiber drawing and extrusion
Precursor fibers were hand drawn or extruded. Hand drawing consisted of dipping a spatula into a viscous solution and withdrawing green fibers, $\leq 30\,\mu$m dia. by 200 mm long. These fibers were suspended from a wooden framework (100×100 mm) and air dried.

Fibers were also extruded in air using the extruder shown in Fig. 1. The extrusion spinneret diameter was $\approx 140\,\mu$m. Typically, 10 ml of precursor solution (ceramic yield ≈ 23 wt%) was loaded into the extruder chamber. Gas pressures, ≈ 300 psi, were used to control the extrusion rate. Because of self-drawing, thicker or thinner fibers could be collected at different distances below the spinneret. The fibers were collected across a square dowel framework below the spinneret. Drawing extruded fibers by moving the square dowel framework gave even thinner continuous fibers. The fibers were also collected using the rotating fiber collector (take up) ≈ 2 m below the spinneret (Fig. 1). Thinner or

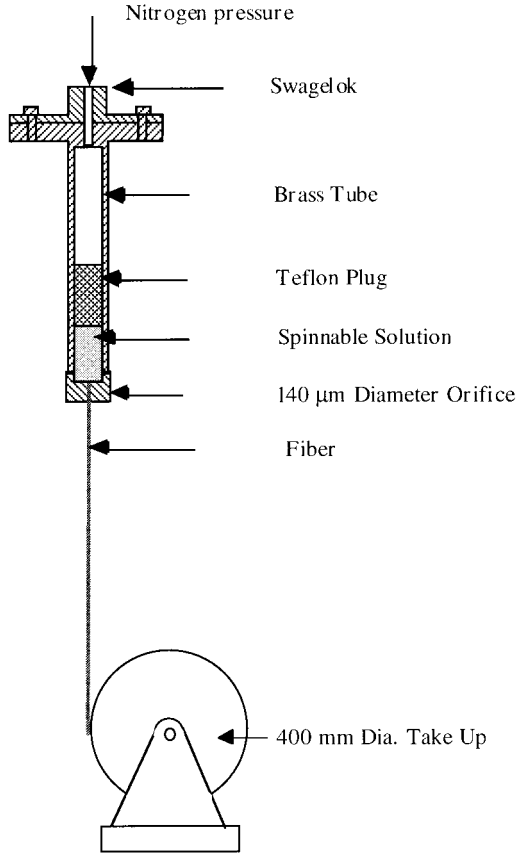

Fig. 1. Precursor fiber extrusion.

thicker fibers were collected with the "take-up" by adjusting its rotation speed. The take-up had a 400 mm dia, and the speed of the take-up rotation was 0–10 rpm. These fibers were taken off the 'collector' as 2–10 cm long fragments and air dried. The thinnest, continuous fibers obtained were $\geq 20\,\mu$m dia.

2.4.2 Pyrolysis studies of fibers

All the spinel precursor fibers were heated at 1°C min^{-1} to 300°C $2\,h^{-1}$ first, then treated to the selected high temperatures. The same Lindberg furnace as used for bulk material studies was used for high temperature pyrolyses. All pyrolyses were conducted in air.

2.4.3 Scanning electron microscopy (SEM)

The appearances of the green and pyrolyzed precursor fibers were examined using a Hitachi S800 scanning electron microscope (SEM. Tokyo, Japan), operating at 5 keV. SEM samples were prepared by mounting precursor fibers (3–5 mm in length) on an aluminum stub using carbon paste. The fibers were sputter coated with $<0{\cdot}1\,\mu$m Au/Pd to improve conductivity.

2.4.4 Fiber bend tests

The strength of pyrolyzed fibers was evaluated using a 'bending test'.[7,14,29–31] The bend strength was calculated using:

$$\sigma = Ez/\rho$$

where E is the elastic modulus (the value used is 280 GPa),[26] z is the shortest distance from the centroidal axis to the surface of the fiber and ρ is radius of curvature at which the fiber breaks.

3 Results and Discussion

In this section, we will discuss (1) the bulk pyrolysis decomposition patterns for Mg acetate hydrate and the spinel precursor, and (2) preliminary studies on fiber processing. The pyrolytic decomposition of Al formate hydrate was discussed recently.[7]

3.1 Characterization of $Mg(O_2CCH_3)_2{\cdot}4H_2O$

3.1.1 Thermal analyses

Based on our previous work on $Y(O_2CCH_3)_3{\cdot}4H_2O$, the thermal decomposition pattern of $Mg(O_2CCH_3)_2{\cdot}4H_2O$ is presumed to proceed via:[32]

$$Mg(O_2CCH_3)_2 4H_2O \xrightarrow{50°-100°C} Mg(O_2CCH_3)_2 + 4H_2O \quad (1)$$

$$Mg(O_2CCH_3)_2 \xrightarrow{\approx 330°C} MgO + MgCO_3(\text{minor}) + [CO_2, H_2O, (CH_3CO)_2O, \text{other}] \quad (2)$$

The TGA profile (Fig. 2) has three major mass loss steps. The first step from room temperature to 85°C, corresponds to the loss of H_2O by hydration. The ceramic yield of the 80°C dried product is 28·8 wt%, close to the calculated value of 28·3 wt% for $Mg(O_2CCH_3)_2$. The second mass loss, occurring between 310 and 330°C, corresponds to oxidative decomposition of the complex. The third step from 330° to 410°C, corresponds to carbonate decomposition (see DRIFTS studies), about 6 wt%.

The DTA (Fig. 3) exhibits endotherms centered at 80°, and 300°C, and exotherms at 330°, 370° and 420°C. The endotherm at 80°C corresponds to loss of H_2O accompanied by sample melting, as $Mg(O_2CCH_3)_2{\cdot}4H_2O$ transforms to $Mg(O_2CCH_3)_2$. At 300°C, $Mg(O_2CCH_3)_2$ melts.[3] Two exotherms centered at 330° and 370°C likely correspond to oxidative decomposition of the organic ligands and then

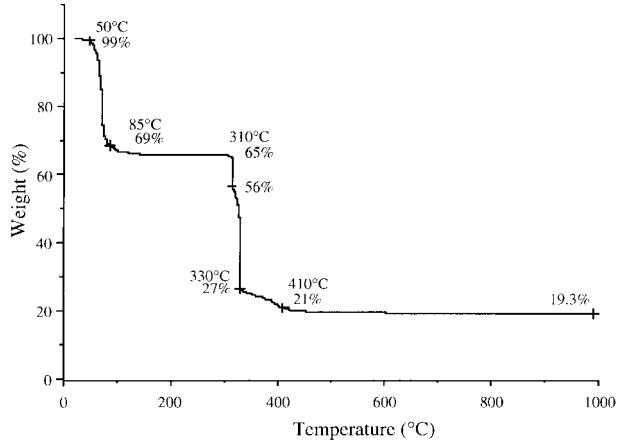

Fig. 2. TGA for $Mg(O_2CCH_3)_2{\cdot}4H_2O$ heated in 'Hi-Res 4·0 mode' at 10°C min^{-1} at 1000°C in air.

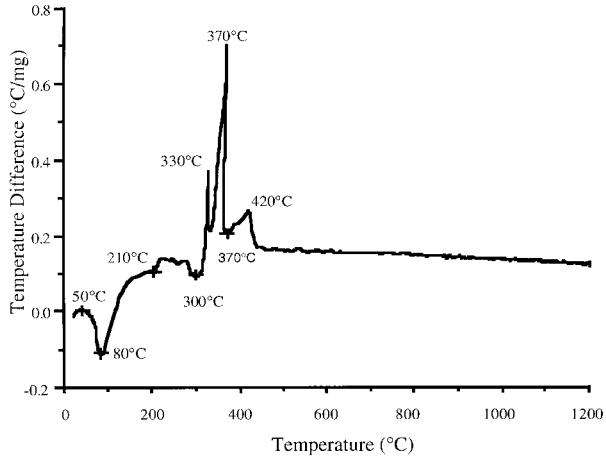

Fig. 3. DTA of $Mg(O_2CCH_3)_2{\cdot}4H_2O$ in air. Sample heated per Fig. 2 at 10°C min^{-1} to 1200°C^{-1}.

char–as suggested in (3) and (4), and as found for decomposition of $Y(O_2CCH_3)_3$ and $Al(O_2CCH_3)_3$:

$$3Mg(O_2CCH_3)_2 \rightarrow Mg_3O(O_2CCH_3)_4+(CH_3CO)_2O \quad (3)$$

$$Mg_3O_2(O_2CCH_3)_2\rightarrow MgO + MgCO_3(\text{minor})+ [CO_2, H_2O, (CH_3CO)_2O, \text{other}] \quad (4)$$

Note that apparatus differences between the TGA and DTA give different temperatures for the same thermal event. Although the TGA and DTA are run with the same heating rate, we encountered problems similar to those in previous studies.[7] In the DTA, the air flows (from below) past the sample pan, so no fresh air flows directly on the sample as in the TGA. Also, the DTA sample pan is deeper than the TGA pan, and appears to form a dead air zone, so less sample surface is exposed to fresh air. Thus, the dead air zone inhibits decomposition. Thus, reactions tend to start at higher temperatures in the DTA.

From 370° to 420°C (Fig. 3), two events occur. One is carbonate decomposition (see DRIFTS section), accompanied by an endotherm (370°C) in the DTA; the other is crystallization of MgO to the rock salt structure (see XRD section). This phase transformation might also contribute to the 420°C exotherm.

3.1.2 Drifts

Figure 4 displays DRIFTS spectra for $Mg(O_2CCH_3)_2$ heated to selected temperatures (10°C min^{-1} air) for 2 h. The DRIFTS studies provide a view of transformations at the atomic scale. The spectrum of $Mg(O_2CCH_3)_2{\cdot}4H_2O$ (Fig. 4) shows weak νO–H bands at 3500–2800 cm^{-1} (due to hydrate H_2O), weak νC–H bands at 3010, and 2960–2950 cm^{-1}, and νC=O bands at 1590, 1440, 1430 and 1350 cm^{-1}. The νO–H bands (3500–2800 cm^{-1}) almost disappear in samples heated to 200°C, indicating elimination of hydrate H_2O as expected from the TGA data.

At 300°C, $Mg(O_2CCH_3)_2$ decomposes and the major peaks change, i.e. the νO–H and νC=O bands are eliminated, and carbonate peaks appear at 1570 and 1450 cm^{-1}. Two new sharp peaks appear at 520 and 440 cm^{-1} (νMg–O), suggesting some crystallization; however this conclusion is not supported by the XRD studies which indicate poor crystallinity for all samples below 1500°C. The sharp IR peaks may be indicative of local ordering only. On further heating, the material

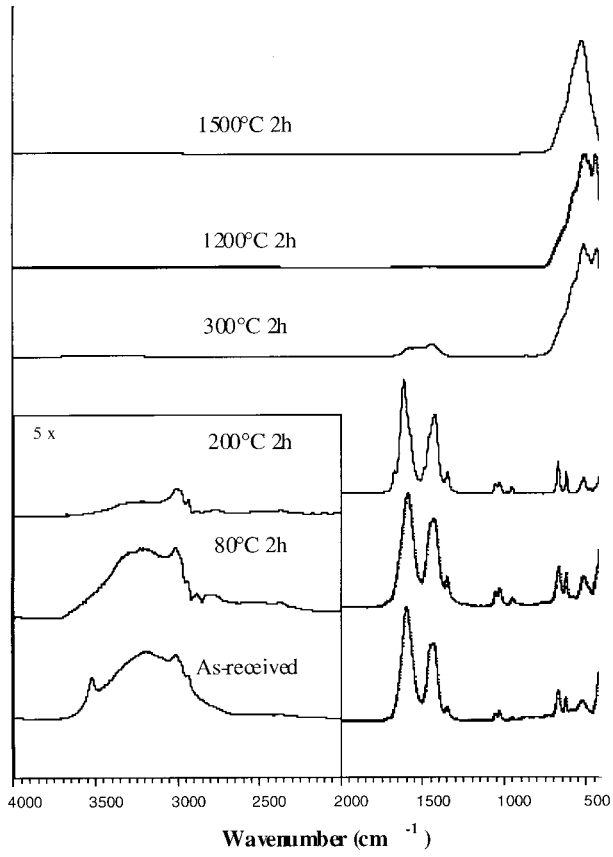

Fig. 4. DRIFT spectra of $Mg(O_2CCH_3)_2{\cdot}4H_2O$ pyrolyzed to selected temperatures. Samples heated at 10°C min^{-1} to selected temperature followed by 2 h hold.

remains unchanged until 1200°C, where the carbonate peaks are eliminated. At 1500°C, the νMg–O bands converge to a single, sharp peak at 530 cm^{-1}, indicating well-crystallized MgO (higher atomic order in better crystallized materials reduces the total number of vibrational modes available, increasing the intensity of the 530 cm^{-1} band).[3]

3.1.3 X-ray powder diffraction (XRD) patterns

Figure 5 displays XRD powder patterns for $Mg(O_2CCH_3)_2{\cdot}4H_2O$ pyrolysis samples produced in the same manner as used in the DRIFTS studies. The as-received sample has an α-Mg acetate hydrate pattern corresponding to JCPDS 14-827. At 200°C, the major phase changes to α-Mg acetate (JCPDS 14-802). The 300°C pattern shows the MgO rock salt structure; however, the broad peaks and poor intensities suggest a nanocrystalline material in accord with the local ordering suggested by the DRIFTS studies. Most of the carbonate decomposes by 600°C, as $<1\%$ mass loss is observed above that (Fig. 2, TGA). The remaining material is assumed to be stoichiometric MgO. At 1500°C, the XRD profile is a well-defined pattern of MgO (JCPDS 4-829) with high relative peak intensities.

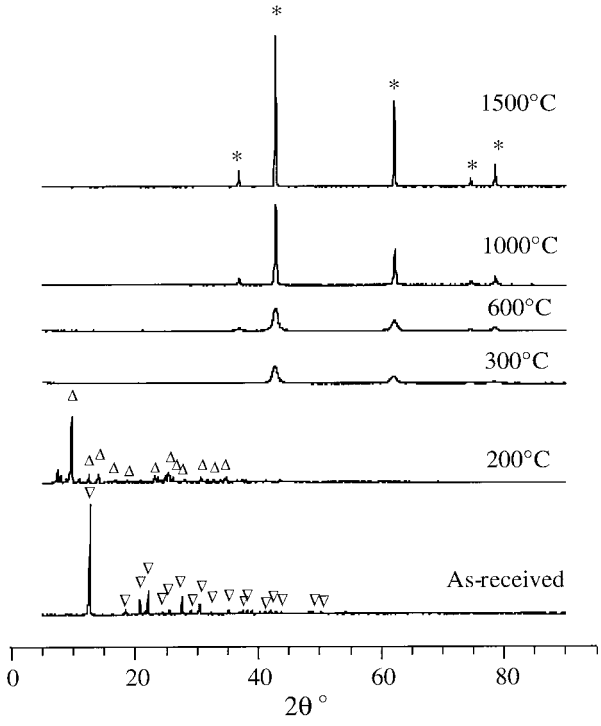

Fig. 5. XRD of $Mg(O_2CCH_3)_2{\cdot}4H_2O$ pyrolyzed to selected temperatures. Samples treated as in DRIFT studies. ▽ corresponds to JCPDS 14-827, α-Mg-acetate hydrate; Δ corresponds to JCPDS 14-802, α-Mg-acetate; * corresponds to JCPDS 4-829, MgO.

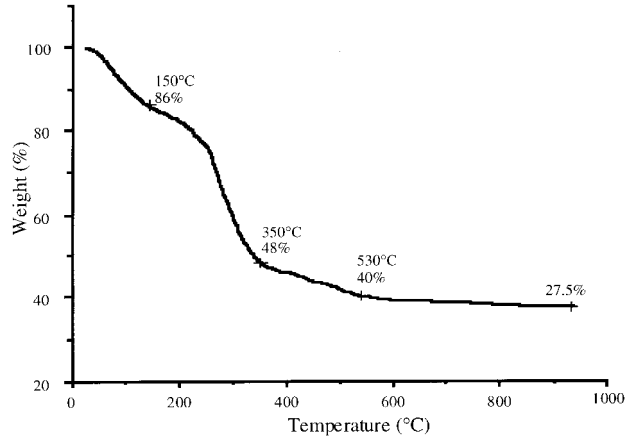

Fig. 6. TGA of spinel precursor heated in 'Hi-Res 4·0 mode' at 10°C min^{-1} to 950°C in air.

Table 1. Possible precursor components and their calculated ceramic yields

Possible precursor components	*Calculated ceramic yield (wt.%)*
$Mg(O_2CCH_3)_2{\cdot}4H_2O{\cdot}2[Al(O_2CH)_3{\cdot}3H_2O]$	22.0
$Mg(O_2CCH_3)_2{\cdot}2[Al(OH)(O_2CH)_2]$	34.7
$Mg(O_2CCH_3)_2{\cdot}2[Al(O_2CH)_3]$	32.5
$Mg(O_2CCH_3)_2{\cdot}2[Al(O_2CH)_3{\cdot}3H_2O]$	31.2
$Mg(O_2CCH_3)_2{\cdot}2[Al(O_2CH)_3]$	30.0

3.1.4 Characterization of the $Mg(O_2CCH_3)_2{:}2Al(O_2CH)_3$, spinel precursor.

This precursor was prepared by dissolution of a $Mg(O_2CCH_3)_2{:}2Al(O_2CH)_3{\cdot}3H_2O$ stoichiometric mixture in H_2O (with small amounts of formic acid, isobutyric acid, and ethylene glycol to stabilize the spinning dope). The formic acid is added to prevent hydrolytic decomposition of $Al(O_2CH)_3$. The isobutyric acid partially exchanges with the formate and/or acetate groups to improve solubility and limit reprecipitation/crystallization of $Al(O_2CH)_3$. The added ethylene glycol raises the solution viscosity to improve spinnability and also to reduce the potential for reprecipitation/crystallization of $Al(O_2CH)_3$. Samples for bulk pyrolysis studies were obtained by vacuum drying and grinding of the spinning dope, using the same procedures as used for the individual compounds.

3.1.5 Thermal analyses

The Fig. 6 TGA profile of the bulk, dry powder shows a found ceramic yield of 27·5% rather than the 22 wt% calculated for the $Mg(O_2CCH_3)_2{\cdot}4H_2O{:}2[Al(O_2CH)_3.3H_2O]$ mixture. This suggests that the precursor does not reflect the components used to formulate it. Table 1 shows the possible precursor components and their combined calculated ceramic yields. Because the DRIFTS data (see below) do not show the strong presence of νO−H, it is clear that the waters of hydration have been removed. Likewise the DRIFTS data do not show the presence of isolated νO−H. Thus, the precursor compound cannot be $Mg(O_2CCH_3)_2{\cdot}2[Al(OH)(O_2CH)_2]$.

It is possible that some formate/acetate exchange occurs during precursor synthesis, resulting in formation of $Mg(O_2CH)_2{\cdot}2[Al(O_2CH)_3]$ (ceramic yield of 32·5%) and/or $Mg(O_2CCH_3)_2{\cdot}2[Al(O_2CH)_3]$ (ceramic yield 30%). A mixture of these two components coupled with trace amounts of isobutyric acid, and ethylene glycol could give the found ceramic yield. Similar carboxylate exchanges appear to also occur during formulation of spinnable YAG formate/acetate precursor solutions.[7] Some acetate ligands probably exchange with the free HCO_2H and/or isobutyric acid used as a stabilizer during precursor synthesis. However, the very low νO−H bands seen in the DRIFTS in Fig. 8 suggest that free acid, water and ethylene glycol, if present in the dry bulk precursor, are present only in low quantities.

Three major mass loss events occur on heating in the TGA (Fig. 6). The first step, 20°–150°C (mass loss 14 wt%), corresponds to loss of H_2O and/or loosely bound organics, suggested by reaction (5) for Al. The second step, from 150 to 350°C (38 wt% mass loss), corresponds to carboxylate ligand

$$Al(O_2CH)_3 3H_2O \xrightarrow{130^\circ C} Al(OH)(O_2CH)_2 0{\cdot}5H_2O + HCO_2H + 0{\cdot}5H_2O \quad (5)$$

decomposition via some or all of the processes shown in reactions (1)–(8). The material turns yellow at this stage.[7]

$$Al(OH)(O_2CH)_2 \xrightarrow{200^\circ C} Al_2O(O_2CH)_4 \quad (6)$$

$$Al_2O(O_2CH)_4 \xrightarrow{270^\circ C} AlO(O_2CH) \quad (7)$$

$$AlO(O_2CH) \xrightarrow{350^\circ C} Al_2O_3 \quad (8)$$

The 480°C mass loss (≈6 wt%) is due to carbonate decomposition. The sample coincidentally turns black at 600°C. Although this process is not seen for the individual compounds, it is seen for the YAG precursor and strengthens the analogies that can be drawn between the two systems.[7] The ≈2% mass loss in the TGA at 790°C results from oxidation of trace amounts of free carbon (samples change from black to white) and carbonate decomposition (see DRIFT section).

In Fig. 7, the DTA shows small endotherms starting at 100 and 230°C (centered at 240°C), and exotherms starting at 310°C (centered at 340°C), 490°C (centered at 510°C), and 775°C (centered at 810°C). The absence of a steep endotherm in the 50–100°C range as seen for $Mg(O_2CCH_3)_2{\cdot}4H_2O$ in Fig. 3, strongly suggests the absence of waters of hydration bound to magnesium. Likewise, the absence of a very sharp endotherm beginning at 90°C[7] also argues against significant waters of hydration bound to aluminum. One might argue that all or some of the waters of hydration have been displaced as supported by the DRIFT spectra discussed below.

To better understand material evolution during pyrolysis, a sample was heated in the DSC in N_2, as shown in the Fig. 7 (inset). Only a slight endotherm is seen in the N_2 DSC at≈100°C that might be attributable to any or all of the volatiles used to formulate the precursor (e.g. free water, formic acid, ethylene glycol or isobutyric acid) all of which have significant vapor pressure above 90°C. The endotherm centered at 240°C (DTA/air, 290°C DSC/N_2) and the exotherm centered at 340°C (DTA/air) correlate with thermal decomposition of carboxylate ligands. The exotherm centered at 510°C (585°C in N_2, see Fig. 7 inset) corresponds to spinel crystallization (see XRD section). The exotherm centered at 810°C corresponds to oxidation of free carbon, as the sample turns from black to white. Note that many of the decomposition processes appear to be quite similar to those seen for YAG, $YBa_2Cu_3O_{7-x}$ and other carboxylate precursors.[7,32,33]

3.1.6 Drifts

Spectra of as-processed spinel precursor, and precursor heated to selected temperatures are shown in Fig. 8. The spectrum of as-processed spinel precursor

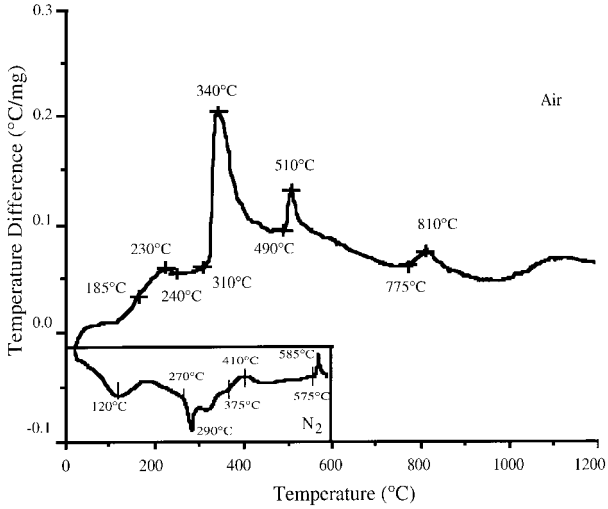

Fig. 7. DTA in air and DSC (inset) in N_2 of spinel precursor. Samples heated at same heating rate as TGA for spinel precursor below 1000°C, and heated at 10°C min^{-1} to 1200°C above 1000°C.

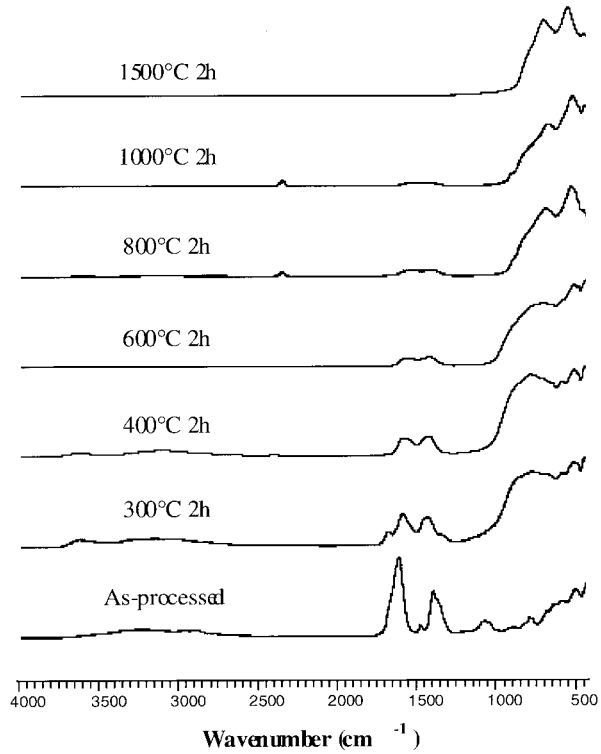

Fig. 8. DRIFT spectra of spinel precursor pyrolyzed to selected temperatures. Samples heated at 10°C min^{-1} to selected temperature followed by 2 h hold.

(bottom) has no common peaks with the IR spectra of the $Mg(O_2CCH_3)_2{\cdot}4H_2O$ and $Al(O_2CH)_3{\cdot}3H_2O$. However, it is similar to that of anhydrous $Al(O_2CH)_3$, but with broader peaks. It is possible that the $Mg(O_2CCH_3)_3{\cdot}4H_2O$ peaks are hidden by $Al(O_2CH)_3{\cdot}3H_2O$ peaks because of the higher concentration of the Al compound, or a new mixed-metal complex forms. As noted above, the peaks attributable to νO–H are low and very broad suggesting trace amounts of carboxylic acids but not waters of hydration or ethylene glycol. Alternately, based on the changes in ceramic yield described above, some acetate ligands were displaced by formate ligands during synthesis of the spinel precursor. The ligand changes are similar to those observed in YAG precursor studies.[7]

At 300°C, the organic ligand peaks disappear and carbonate peaks centered at 1580 and 1430 cm^{-1} appear, indicating that the carboxylate ligands decompose to carbonate and oxide. A weak νO–H peak at 3600 cm^{-1} indicates isolated surface hydroxyl groups, which might result from a reaction between carbonate or oxide and H_2O, an oxidation byproduct. A weak but broader νO–H band centered at $\approx$3150 cm^{-1} represents either physisorbed H_2O or hydrogen-bonded O–H groups on the surface, which might also form during thermal decomposition. The O–H peaks disappear at 600°C. The carbonate peaks persist to only 800°C. At 600°C, peaks at 510 (νMg–O) and 700 (νAl–O) cm^{-1} appear, indicating the appearance of crystalline spinel (see XRD section).[34,35] At 1500°C, the peaks shift to 560 and 750 cm^{-1}, and sharpen, indicating well-defined crystalline spinel.

3.2 X-ray powder diffraction patterns

XRDs of bulk pyrolysis samples are shown in Fig. 9 No intermediate crystalline phases, e.g. rock salt MgO, η or α-alumina, are observed before crystallization of spinel, which starts at $\approx$600°C (from XRD). Above 600°C, continued refinement in peak shapes and intensities indicate grain growth of crystalline spinel as temperature increase.

3.3 Fiber processing

Because of the extreme changes in volume and density that occur as a green, precursor fiber is transformed into a ceramic fiber during pyrolysis, the heat treatment schedule must be carefully designed to successfully process fully dense, defect free, polycrystalline spinel fibers, as discussed below.

3.3.1 Density and volume changes

The density of cold, compacted disks of dried spinel precursor (see experimental) is $1{\cdot}6 \pm 0{\cdot}01$ g cc^{-1}, while the reported density of spinel is 3·6 g cm^{-3}.[26]

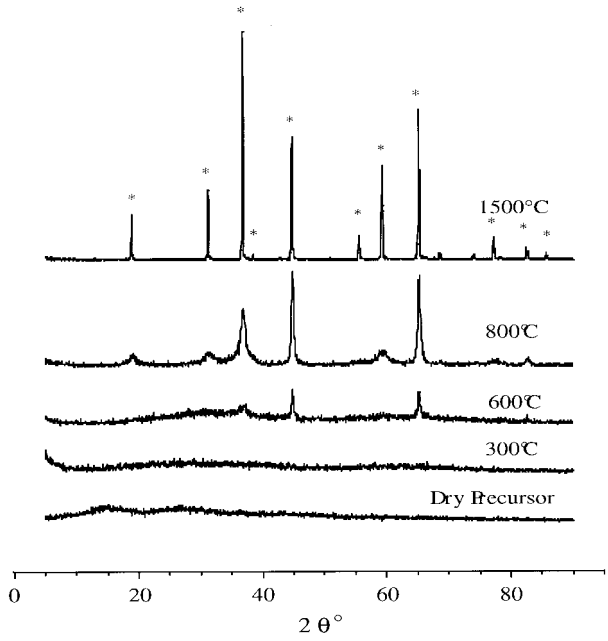

Fig. 9. XRD of spinel precursor pyrolyzed to selected temperatures. Samples treated as in DRIFT studies. * Corresponds to JCPDS 21-1152, spinel.

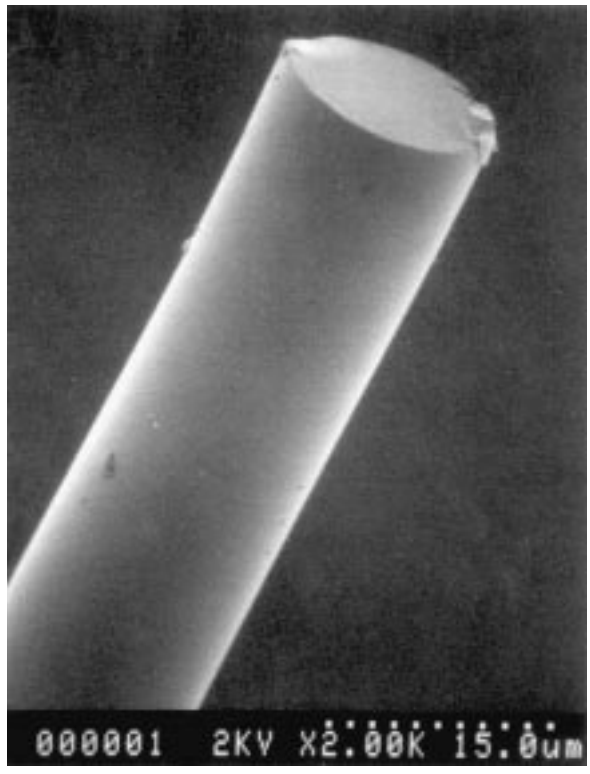

Fig. 10. SEM of as-spun extruded spinel precursor fiber.

The theoretical volume change resulting from both mass loss and densification is 88%. If the volume change in fully dense precursor fibers occurs only in the diametrical dimension, the expected change in diameter will be 65%, if full densification is obtained. The 88% volume change and the release of gaseous products are the main reasons for loss of fiber integrity during transformation of green

fiber to ceramic fiber. Thus, slow heating rates during carboxylate decomposition are necessary to control gas evolution.

3.3.2 Preliminary studies of fiber processing
Based on our YAG fiber processing experience, we focused on producing thin spinel fibers (dia. $\leq 20\,\mu$m).[7] Fig. 10 is a SEM micrograph of an extruded green fiber. The 15 μm diameter, as-spun fiber has a circular cross-section and a smooth surface. After heating at 1°C min^{-1} to 300°C 2 h^{-1} in air to remove carboxylate ligands, the fibers appear dense as no pores or cracks are observed (Fig. 11). Above 300°C, the fibers were continuously heated at 15°C/min to temperatures higher than 800°C. Figure 12 shows a cross section of a fiber heated to 800°C/2 h. The fiber does not appear fully dense as the texture suggests a porous material. Figures 13 and 14 show SEMs of fibers heated to 1000° and 1200°C 2 h^{-1} respectively. Although some process related pores are visible, no distinct features are observed as the fiber cross-section looks dense and the skin is smooth. Compared to previous studies on YAG fibers,[7] which exhibit a porous structure at the same sintering temperature, the pores in the spinel fibers, if any, are much smaller. At 1500°C, the average grain size is $1{\cdot}2 \pm 0{\cdot}4\,\mu$m and dense spinel fibers ($\approx 10\,\mu$m in dia.) are obtained (Fig. 15).

3.3.3 Mechanical properties of spinel fibers.
Room temperature fiber strength was estimated using a bending test. The bend strengths of 1500°C^{-1} 2 h^{-1} in air pyrolyzed fibers were evaluated, as described in the experimental section. A

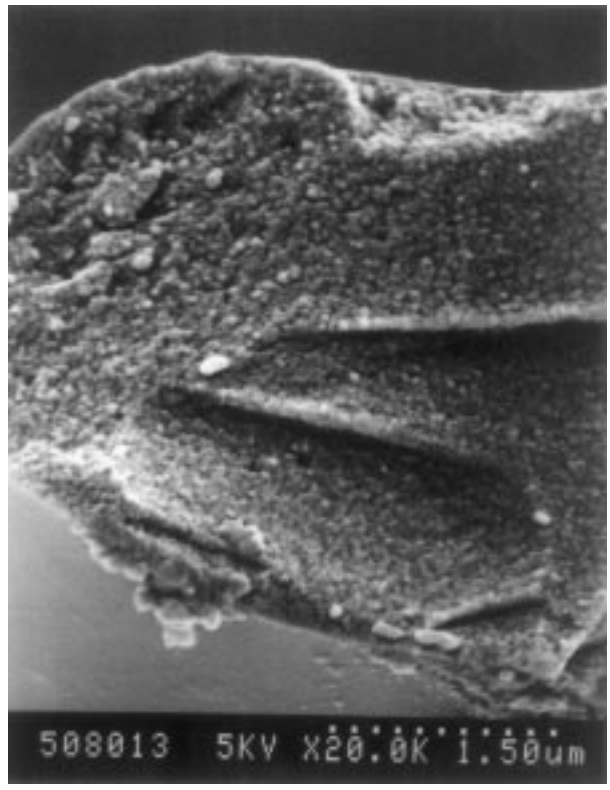

Fig. 12. SEM of extruded spinel precursor fiber heated at 1°C min^{-1} 300°C 2 h^{-1}, then 15°C min^{-1} 800°C 2 h^{-1}.

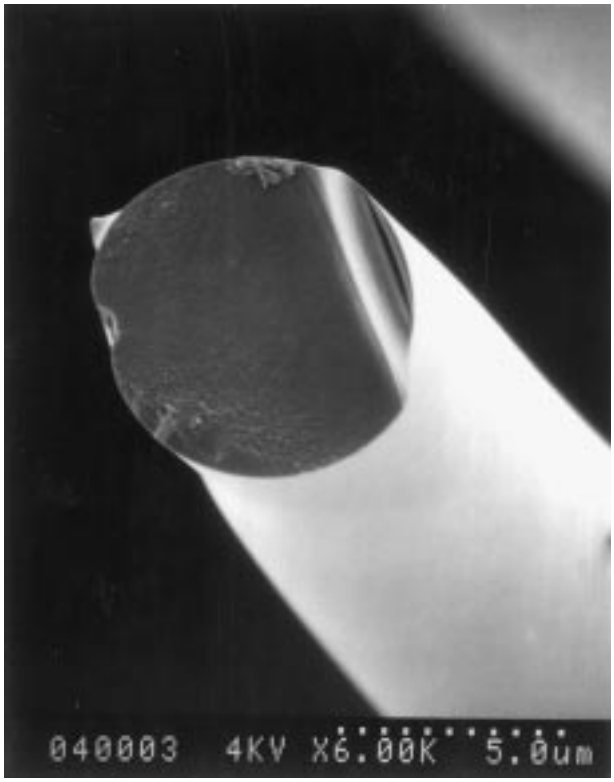

Fig. 11. SEM of extruded spinel precursor fiber heated at 1°C min^{-1} to 300°C for 2 h.

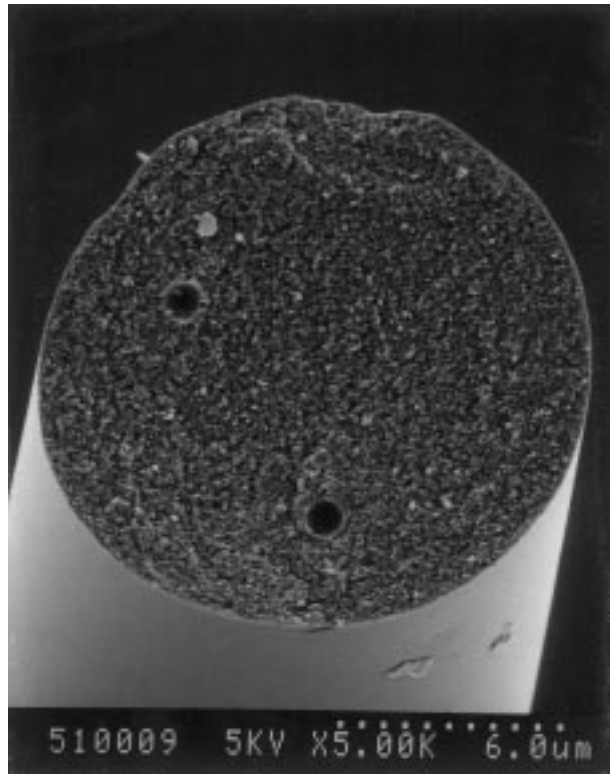

Fig. 13. SEM of extruded spinel precursor fiber heated as in Fig. 12 to 1000°C 2 h^{-1}.

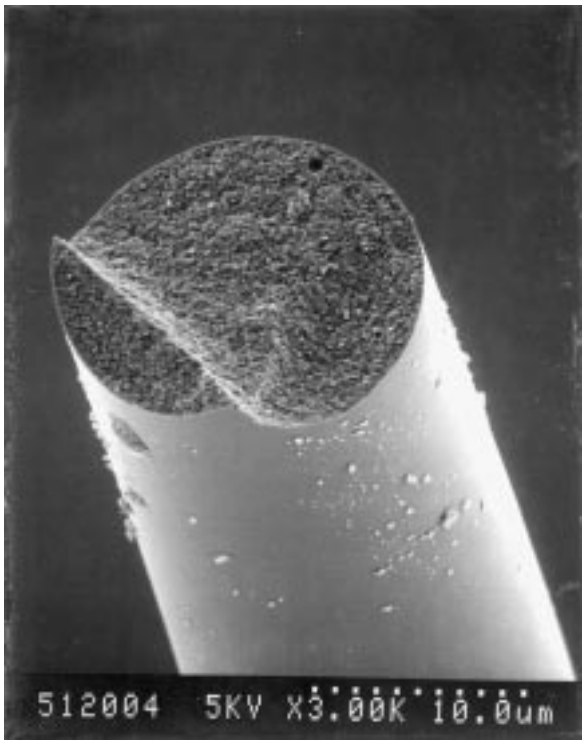

Fig. 14. SEM of extruded spinel precursor fiber heated as in Fig. 12 to 1200°C $2\,h^{-1}$.

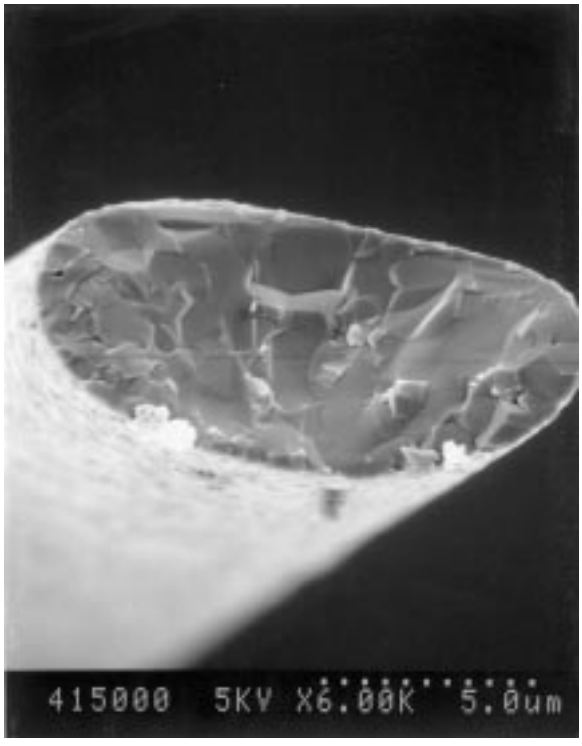

Fig. 15. SEM of extruded spinel precursor fiber heated as in Fig. 12 to 1500°C $2\,h^{-1}$.

total of 12 fibers were used. SEM reveals almost fully dense fiber cross-sections (Fig. 15). Although several tiny pores can be observed, the pore fraction is less than 0·5%, evaluated via linear line fraction analyses. Most of the fractures of 1500°C sintered fibers are transgranular, indicating the grain strength is $\leq$ grain boundary strength. The

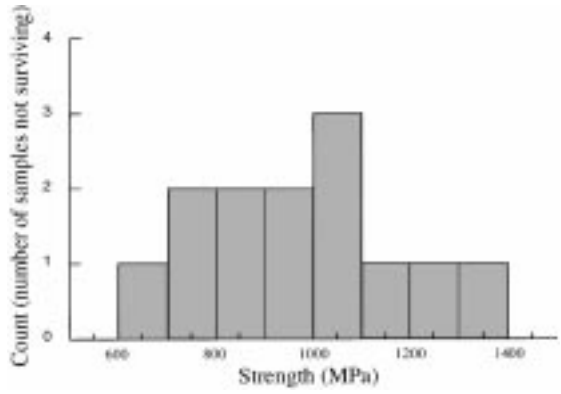

Fig. 16. Strength distribution of spinel fibers.

average strength of the fibers ($\approx 10\,\mu m$ dia.) is $1{\cdot}0 \pm 0{\cdot}4$ GPa. The calculations assume that the fibers tested are fully dense, have the same density and use the bulk elastic modulus of 280 GPa. Figure 16 shows, for the limited number of samples, a normal strength distribution of the tested fibers. The room temperature strength of spinel fibers is lower than commercial Nextel 610 alumina fiber (10–12 μm dia., tensile strength $\approx 2{\cdot}8$ GPa, grain size $\langle 0{\cdot}5\,\mu m$) with similar diameter. Two reasons contribute to the lower strength. One is the different strength test methods, e.g. tensile test versus bending test (note that bend strengths are typically higher). But perhaps the most important reasons are flaw population and grain size differences. The grain size of spinel fibers (1500°C sintering) is $\geq$ 10 times the grain sizes of Nextel 610 fibers (not heated to 1500°C), thus the spinel fibers offer lower strength.

4 Conclusions

The chemical evolution that occurs during the pyrolytic transformation of bulk samples of $Mg(O_2CCH_3)_2{\cdot}4H_2O$ to rock salt magnesia ($\geq$ 300°C) was examined. These results and previous studies on the pyrolysis behavior of $Al(O_2CH)_3{\cdot}3H_2O$ established basic behavior patterns for evaluating the decomposition patterns of a spinel precursor formulated from 1:2 stoichiometric mixtures of $Mg(O_2CCH_3)_2{\cdot}4H_2O$ and $Al(O_2CH)_3{\cdot}3H_2O$ dissolved in H_2O with stabilizing additives, and recovered by vacuum evaporation of solvent. The spinel precursor behaves like a separate compound and decomposes to crystalline spinel directly at $\approx$600°C, without any conclusive evidence of phase separation.

Finally, the spinel precursor was easily extruded or hand drawn to form well-defined green fibers. The 20 μm dia., extruded fibers were pyrolyzed at 300°C $2\,h^{-1}$ in air to remove carboxylate ligands, and then sintered at 15°C min^{-1} to 1500°C $2\,h^{-1}$ in air. The final fibers are $\approx 10\,\mu m$ in dia. with $1{\cdot}2 \pm 0{\cdot}4\,\mu m$ grain sizes and offer an average bend

strength of $1{\cdot}0 \pm 0{\cdot}4$ GPa. The larger grain size of spinel fiber may contribute to the lower strengths compared with commercial alumina fibers (not heat treated to 1500°C) with similar diameters.

Acknowledgements

We would like to thank the US Air Force Wright Laboratory, Wright Patterson Air Force Base for generous support of this work through Contract Nos. F33615-91-C-5650, FQ8671-9700732 and the Office of Naval Research for partial support.

References

1. Romine, J. C., Aluminum oxide fibers. In *Handbook of Fiber Science and Technology*: Volume III, *High Technology Fibers Part B*, ed. M. Lewin and J. Preston, Marcel Dekker, Inc., New York, 1983, pp. 151–175.
2. Johnson, D. D., *J. Coated Fabr*., 1981, **11**, 282.
3. Everitt, G. F., Stabilized aluminum acetate used for an alumina source in ceramic fibers. In *Ultrastructure Processing of Advanced Ceramics* ed. J. D. Mackenzie and D. R. Ulrich. John Wiley and Sons, New York, 1988.
4. Sowman, H. G. and Tran, T. T., Refractory fibers of alumina and amorphous phosphorus pentoxide. US Patent No. 4,801, 562, 1989.
5. Wood, T. E. and Wilson, D. M., Microcrystalline alumina-based ceramic articles. U. S. Patent No. 4,954, 462, 1990.
6. (a) Sowman, H. G., Refractory fibers of alumina and organic residue. U. S. Patent No. 4,929,578, 1990. (b) Wilson, D. M., Lueneburg, D. C. and Lieder, S. L., High temperature properties of nextel 610 and alumina-based nanocomposite fibers. *Ceram. Eng. Sci. Proc*., 1993, **14**(7–8), 609–621.
7. Liu, Y., Zhang, Z-F., Halloran, J. and Laine, R. M., Yttrium aluminum garnet fibers from metallo-organic precursors. *J. Am. Ceram*., 1998, **81**, 629–645.
8. (a) Chen, L., Wang, B., Liu, S. and Yan, Y. Preparation of mullite fiber. *J. Am. Ceram. Soc*., 1996, **79**(6), 1494–1498 (b) Marshall, D. B., Lange, F. F. and Morgan, P. E. D. High-strength zirconia fibers. *J. Am. Ceram. Soc*., 1987, **70**(8) C187–C188. (c) Fernandez, M. E. P., Kang, C. and Mangonon, P. L. Processing ceramic fibers by sol–gel. *Chem. Eng. Prog*., 1993, **9**, 49–53. (d) Emig, G., Wirth, R. and Zimmermann-Chopin, R. Sol/gel-based precursors for manufacturing refractory oxide fibers. *J. Mater. Sci*., 1994, **29**, 4559–4566.
9. Morscher, G. N., Chen, K. C. and Mazdiyasni, K. S., Creep-resistance of developmental polycrystalline yttrium-aluminum garnet fibers. *Ceram. Eng. Sci. Proc*., 1994, **14**(7–8), 181–188.
10. King, B. H., Liu, Y., Laine, R. M. and Halloran, J. W., Fabrication of yttrium aluminate fibers. *Ceram. Eng. and Sci. Proc*., 1993, **14**(7–8), 639–650.
11. (a) Yang, J., Jeng, S. M. and Chang, S. Fracture behavior of directionally solidified $Y_3Al_5O_{12}/Al_2O_3$ eutectic fiber. *J. Am. Ceram. Soc*. 1996 **79**(5) 1218–1222. (b) Mah, T., Parthasarathy, T. A. and Matson, L. E. Processing and properties of $Al_2O_3/Y_3Al_5O_{12}$ (YAG) eutectic composite. *Ceram. Eng. Sci. Proc*., 1990, **11**(9–10), 1617.
12. (a) Tissue, B. M., Jia, W., Lu, L. and Yen, W. M. Coloration of chromium-doped yttrium aluminum garnet single-crystal fibers using a divalent codopant. *J. Appl. Phys*. 1991, **70**(7) 3775–3777. (b) Corman, G. S. Strength and creep of single crystal YAG fibers presented at the 94th Annual Meeting of the American Ceramic Society, Minneapolis, MN, 12–16 April, 1992.
13. (a) Wallenberger, F. T., Weston, N. E. and Dunn, S. A. Inviscid melt spinning: as-spun crystalline alumina fibers. *J. Mater. Res*., 1990, **5**(11), 2682–2686. (b) Wallenberger, F. T., Weston, N. E., Motzfeldt, K. and Swartzfager, D. G. Inviscid melt spinning of alumina fibers: chemical jet stabilization. *J. Am. Ceram. Soc*., 1992, **75**(3) 629–636. (c) Melt spinning of amorphous alumina fibers. information provided by Wallenberger, F. T. *Am. Ceram. Soc. Bull*., 1990, **69**(10), 1646–1648.
14. King, B. H. and Halloran, J. W., Polycrystalline yttrium aluminum garnet fibers from colloidal sols. *J. Am. Ceram. Soc*., 1995, **78**(8), 2141–2148.
15. Cooke, T. F., Inorganic fibers-a literature review. *J. Am. Ceram. Soc*., 1991, **74**(12), 2959–2978.
16. Chaim, R. and Talanker, V., Microstructure and mechanical properties of SiC platelet/cordierite glass–ceramic composites. *J. Am. Ceram. Soc*., 1995, **78**(1), 166–172.
17. Jang, H. M., Surface precipitation route for the development of cordierite–zirconia composites. *J. Am. Ceram. Soc*., 1995, **78**(3), 723–727.
18. Genevrier, M. and Mocellin, A., Reaction sintering and mechanical behavior of cordierite containing sapphirine dispersoids. *J. Am. Ceram. Soc*., 1996, **79**(8), 2098–2104.
19. Kingery, W. D., Bowen, H. K. and Uhlmann, D. R. *Introduction to Ceramics*. 2nd ed. Wiley, New York, 1976, p. 755.
20. Hyun, S. H. and Song, W. S., Duplex spinel-ZrO_2 ceramics. *J. Mater. Sci*., 1996, **31**, 2457–2460.
21. Dudek, H. J., Borath, R. and Kleine, A., Spinel growth in the interface of δ-Al_2O_3 fiber reinforced aluminium piston alloys. *J. Mater. Sci*., 1996, **31**(1), 795–805.
22. Evans, R. M., Magnesia-alumina-spinel raw materials production and preparation. *Am. Ceram. Soc. Bull*., 1993, **72**(4), 59–63.
23. (a) Baudin, G., Martinez, R. and Pena, P. High-temperature mechanical behavior of stoichiometric magnesium spinel. *J. Am. Ceram. Soc*., 1995, **78**(7), 1857–1862. (b) Panda, P. C., Raj, R. and Morgan, P. E. D. Superplastic deformation in fine-grained $MgO{\cdot}2Al_2O_3$ spinel. *J. Am. Ceram. Soc*., 1985, **68**(10), 522–529.
24. Sindel, M., Travitzky, N. A. and Claussen, N., Influence of magnesium-aluminum spinel on the directed oxidation of molten aluminum alloys. *J. Am. Ceram. Soc*., 1990, **73**(9), 2615–2618.
25. Lepkova, O., Batarjav, A., Samuneva, B., Ivanova, Y. and Georgieva, L., Preparation and properties of ceramics from magnesium spinel by sol–gel technology. *J. Mater. Sci*., 1991, **26**, 4861–4864.
26. Richerson, D. W., Modern ceramic engineering. Marcel Dekker, Inc., New York, 1992, p. 166.
27. Sheehan, J. E., Sigalovsty, J., Haggerty, J. S. and Porter, J. R., Mechanical properties of $MgAl_2O_4$ single crystal fibers. *Ceram. Eng. Sci. Proc*., 1993, **14**(7–8), 660–670.
28. Sigalovsty, J., Wills, K. C., Haggerty, J. S. and Sheehan, J. E., Growth, characteristics and properties of spinel single crystal fibers. *Ceram. Eng. Sci. Proc*., 1992, **13**(7–8), 183–189.
29. Liu, Y., Zhang, Z.-F., King, B., Halloran, J. W. and Laine, R. M., Synthesis of yttrium aluminum garnet from yttrium and aluminum isobutyrate precursors. *J. Am. Ceram. Soc*., 1996, **79**(2), 385–394.
30. Zhang, Z.-F., Kennish, R. A., Blohowiak, K. A., Hope, M. L. and Laine, R. M., Superconducting fibers from organometallic precursors. Part III. High temperature pyrolytic processing. *J. Mater. Res*., 1993, **8**, 1777–1790.
31. Siemers, P. A., Mehan, R. L. and Moran, H., A comparison of the uniaxial tensile and pure bending strength of SiC filaments. *J. Mater. Sci*., 1988, **23**, 1329–1333.
32. Maksimov, V. N., Semenenko, K. N., Naumova, T. N. and Novoselova, A. V., The aluminium acetates. *Russian J. Inorg. Chem*., 1960, **5**(3), 267–270.
33. Lange, N. A., *Handbook of Chemistry*, 4th ed. McGraw-Hill Book Company, Inc., New York, 1961, p. 266.
34. Kansal, P. Novel chemical routes to ceramics from precursors. Ph. D. dissertation, Dept. of Mater. Sci. and Eng., University of Michigan, 1996.
35. Waldner, K., Laine, R. M., Bickmore, C., Dumrongvaraporn, S. and Tayaniphan, S., Synthesis, processing and pyrolytic transformation of a spinel polymer precursor made from MgO and $Al(OH)_3$. *Chem. Mater*., 1996, **8**, 2850–2857.